ELECTROCAM: ASSESSING THE EFFECT OF LOW-THRUST UNCERTAINTIES ON ORBIT PROPAGATION

M. Maestrini[(1)], A. De Vittori[(1)], J. L. Gonzalo Gómez[(1)], C. Colombo[(1)], P. Di Lizia[(1)], J. Míguez Arenas[(2)], M. Sanjurjo Rivo[(2)], A. Diez Martín[(3)], P. Gago Padreny[(3)], and D. Escobar Antón[(3)]

[(1)]*Politecnico di Milano, 20133 Milan, Italy, Email: {michele.maestrini, andrea.devittori, juanluis.gonzalo, camilla.colombo, pierluigi.dilizia}@polimit.it*
[(2)]*Universidad Carlos III de Madrid, 28911 Madrid, Spain, Email: {joaquin.miguez, manuel.sanjurjo}@uc3m.es*
[(3)]*GMV, 28760 Tres Cantos, Madrid, Spain, Email: {adiez, pau.gago.padreny, descobar}@GMV.com*

ABSTRACT

In recent years low-thrust propulsion has become an alternative to chemical propulsion for many different applications. Hence, it becomes necessary to have accurate and fast methods to improve the uncertainty realism of the propagated orbits to improve the measurement correlation process and to allow a more accurate estimation of collision probabilities. To tackle this problem, many different techniques for orbital uncertainty propagation have been developed in recent years. This work proposes an analysis of several uncertainty propagation methods belonging to different families of methods (i.e., dynamics-based and probabilistic) leveraging different techniques (e.g., Differential Algebra, Gaussian Mixture Models, Kernel Density Estimators, Spherical Radial Cubature, and Unscented Transform). The results of the application of the presented methods across a wide spectrum of missions are presented in this work. The implemented techniques and scenarios have been developed in the framework of the ESA-funded ELECTROCAM contract.

Keywords: Low-Thrust; CAM; Collisions; Uncertainty.

1. INTRODUCTION

In recent years low-thrust propulsion has become a credible alternative to standard chemical propulsion for many different applications, ranging from orbital transfers to day-to-day operations of small satellites in LEO [1]. Indeed, this latter case is gaining a growing interest owed to the advent of mega-constellations endowed with a miniaturized propulsion system capable of granting control authority to such a class of satellites [2]. Despite the extensive effort that has been put into development of guidance algorithms relying on low-thrust propulsion, only few works have focused on the analysis of collision avoidance for such missions[3, 4]. This task is not only impacted by the standard uncertainty in the orbital dynamics model, but also by the stability of thruster performance. Actually, this aspect must be factored-in when computing state uncertainties in order to adequately estimate the collision probability. Besides, the adoption of low-thrust also affects the time needed for corrective actions due to the reduced control authority that leads to longer thrusting arcs. This in turn impacts the achievable risk reduction or the selection of a suitable threshold in terms of accepted collision probability level [5]. Moreover, the accuracy of the computed Probability of collision (PoC) strongly impacts decision making by mitigating collision risk or by avoiding unnecessary Collision Avoidance Maneuvers (CAM) execution.

In light of these considerations it becomes a pressing issue to accurately quantify state uncertainties under the effect of low-thrust noise in a timely manner. In particular, the adoption of continuous thrust for long arcs may strongly affect the propagation of the statistics with respect to a pure ballistic motion. Hence, it is paramount to select an uncertainty propagation strategy that can deal with the actual performance of the thrusters, managing high-frequency thrust variations, thrust interruptions, and uncertain command execution times. In fact, these effects, coupled with the nonlinear dynamics and the orbital uncertainties mapping, sway the validity of the standard Gaussianity assumption adopted by state-of-the-art methods. In order to address the most general and accurate case of uncertainty propagation, one can solve the problem that stems from the Itô stochastic differential equation [6]

$$d\mathbf{x}(t) = \mathbf{f}(\mathbf{x}, t)dt + \mathbf{G}(t)d\boldsymbol{\beta} \tag{1}$$

where $\mathbf{x} \in \mathbb{R}^n$ is the random state vector, $\boldsymbol{\beta}(t) \in \mathbb{R}^m$ is an m-dimensional Brownian motion process with zero mean and covariance $\mathbf{Q}(t)$. The vector function $\mathbf{f}(\mathbf{x}, t)$ captures the deterministic part of the dynamics, and $\mathbf{G}(t)$ is an $n \times m$ matrix characterizing the diffusion. For a given dynamical system that satisfies the Itô stochastic differential equation, the probability density function time evolution can be described by the Fokker–Planck partial differential equation (FPE) [7]. However, solving

a FPE in orbital mechanics is a difficult task, due to its high dimensional state–space and its underlying highly nonlinear dynamics [8]. Alternatively, to retrieve a complete statistical description, one may carry out computationally expensive particle-type studies such as Monte Carlo (MC) simulation [9]. However both methods have a considerable computational cost, owing to the entire statistical description of a trajectory. To address this issue, many analytical or semi-analytical techniques for orbital uncertainty propagation have been developed in recent years [10].
By assuming Gaussian uncertainties and by further performing a local linearization of the dynamics (LinCov) [11] or a linearization in an "average" sense (CADET) [12], linear methods can completely characterize the propagated distributions. While these formulations are simple and efficient, their accuracy drops off for highly nonlinear systems, long-duration uncertainty simulations, or large initial uncertainty.
Several nonlinear techniques have been proposed in literature to refine the uncertainty realism. Probabilistic methods infer statistical properties from the propagation of a deterministically selected (small) number of samples (e.g., Unscented Transform [13], Cubature methods [14], Polynomial Chaos expansion [15]). On the other hand, dynamics-based procedures such as the state transition tensors (STTs) [16] were designed for motion approximation through higher order Taylor series expansion [17]. However, this method may require a significant computational effort to extract the required partials for high-fidelity dynamic systems. Thanks to automatic differentiation provided by differential algebra (DA) [18], the disadvantages of STTs methods can be overcome [19]. Indeed, DA provides a flexible tool that can be leveraged in many different ways to propagate uncertainties with lessened computational burden: polynomial evaluations initial distributions (i.e., MC-like), Isserlis' formula (i.e., STT-like approach without the computational effort), linear propagation (i.e., LinCov-like).[19] Nonetheless, none of the described strategies can deal with the high-order uncertainty propagation with low-thrust noise in a timely manner. This is indeed a particularly daunting task as the introduction of process noise results in a massive (in principle infinite) increase in the number of uncertain variables and the need to assess their effect along the trajectory with ad-hoc methods [20]. Typically, thrust noise is accounted for a covariance inflation term after propagation. However, this approach disregards any effect of noise on higher order moments of the statistics, as well as any coupling between uncertainty in the initial state and in the thrust. In addition, even by assuming perfect propagation of the uncertainty, any nonlinear transformation warps the Gaussian shape of a distribution; hence, it becomes necessary to provide a different description of the uncertainty. A possible solution is to describe the final uncertainty with Gaussian mixture models (GMM) [21, 22, 23]. The key concept behind GMM is to separate a large domain into many smaller subdomains, represented with Gaussian mixture elements (GMEs), on which the dynamics can be linearized. The weights combining GMEs can then be determined both statically [22] as well as dynamically during propagation [21].

To tackle all of these challenging aspects while providing a computationally efficient approach, this work investigated several different methods belonging to both dynamics based methods, as well as probabilistic based approaches.

The former methods rely on carefully mixing GMM with DA, which has been proved effective for uncertainty quantification as well as for PoC computation for problems without low-thrust [24, 25, 23] The first technique is called Adaptive Differential Algebraic Gaussian Mixture Model (ADAGMM), and the peculiarity of this technique is that a nonlinearity index is computed during the propagation of each GME, effective to understand whether it is necessary to adaptively split the element to avoid the onset of nonlinearity. Besides providing automatic partials (which are useful for nonlinearity and split computations), DA also provides the state transition maps necessary to include the thrust noise during propagation. The second proposed method is the Stochastic Taylor Model (STM): a DA extension that endows the ODE flow expansion of the final state with an expansion of the embedded covariance inflation linked to the process noise. After propagating these two polynomial maps the final distribution of states can be retrieved. A GMM can then be fit to this distribution and the polynomial map of the covariance inflation is evaluated at the location of the GMM's means to retrieve the covariance correction term. By combining these two components, the final probability distribution is obtained as a GMM.

On the other hand, probabilistic methods consider stochastic dynamic models that allow us to include the thrust uncertainty in a seamlessly manner. A time-dependent uncertainty model for both thrust acceleration and pointing is proposed. The integration of the resulting stochastic differential equations is done using a stochastic Runge-Kutta, compatible with the thrust uncertainty model. The uncertainty propagation, in turn, is performed using Unscented Transform (UT), cubature schemes such as the Spherical Radial Cubature (SRC) and Kernel Density Estimator (KDE) methods.

The next section will be dedicated to a thorough description of the developed methods. Subsequently, a following section will be dedicated to the description of the study cases. Furthermore, this work will present a numerical assessment of the proposed approaches in terms of both accuracy of the uncertainty propagation as well as on their usage and effect on PoC computation.

2. DYNAMICS-BASED UNCERTAINTY PROPAGATION

This section presents the description of the two dynamics-based UP advanced methods proposed in this work. Such methods combine the benefits of automatic differentiation native to DA techniques with the capa-

bility to deal with simplified linearized models typical of GMM [26]. Before diving into the specifics of each method, it is necessary to provide a brief introduction to DA and its benefits.

2.1. Expansion of ODE flow with DA

DA brings the treatment of functions and the operations on them to the computer environment in a similar way as the treatment of real numbers as presented in [18]. The implementation of DA in a computer allows to compute the Taylor coefficients of a function up to a specified order k in a fixed amount of effort, and it can be used to perform composition of functions, to invert them, to solve nonlinear systems explicitly, to differentiate, and to integrate.
Given a general set of ODEs described by:

$$\dot{\mathbf{x}} = \mathbf{f}(t, \mathbf{x}, \mathbf{u}) \tag{2}$$

The main advantage of DA is that, by setting the initial state as a DA variable and by carrying out all the evaluations in the DA environment, it is possible to retrieve the arbitrary order expansion of the flow of such set of ODEs with respect to variations of the initial condition as

$$[\mathbf{x}_f] = \mathbf{x}_f + \mathcal{T}^N_{\mathbf{x}_f}(\boldsymbol{\delta}\mathbf{x}_0) \tag{3}$$

After integrating the ODEs, the result of the final step of integration is a constant coefficient of the nominal propagated state $\mathbf{x}_f$ plus a N-th order Taylor expansion of the flow expressed in terms of variation of the initial state $\boldsymbol{\delta}\mathbf{x}_0$ at the final time t_f: $\mathcal{T}^k_{\mathbf{x}_f}(\boldsymbol{\delta}\mathbf{x}_0)$. DA techniques were developed for the ESA in the C++ DACE library by Dinamica Srl [27].

2.2. Adaptive Differential Algebraic Gaussian Mixture Model

This approach assumes that a Gaussian distribution remains Gaussian under a linear transformation and that any regular nonlinear transformation behaves almost linearly if the domain of interest is sufficiently small. Suppose to have a Gaussian distribution at an initial time t_0, owing to a non-linear dynamics propagation the covariance is inflated and distorted over time. To overcome this issue, the ADAGMM method is conceived to split the original GME into an increasing number of GMMs as the dynamics are forwardly propagated through a DA based nonlinearity index. The routine is organized in this way:

1. Initialization of the GMM at time instant t_0, this case also includes the simple one of a single GME with weight 1 for the initial distribution, but also allows to propagate GMMs directly.
2. Each GME is added to a list of elements that need to be propagated until t_f and the propagation module starts to propagate each of them.
3. The propagation of mean and covariance is carried out both at first and at second order and at each step a nonlinearity metric is computed to detect the onset of nonlinearity (i.e., the need to further split uncertainty).
4. If the propagation threshold is not violated, the element is propagated until the end of the time window. Otherwise, a univariate splitting library [23] is applied to split the element in a set of new GMEs which are added to the list of elements that still need propagation, and the algorithm goes back to step 2.

When the propagation finishes for all GMEs, the final GMM can be assembled.
By calling t_0 the initial propagation time of a given GME, it is possible to characterize this distribution through an initial mean $\mathbf{x}_0$, covariance $\mathbf{P}_0$, and weight w_0. If the mean state is initialized as a DA variable and if the numerical integration of the ODEs describing the dynamics are carried out in a DA environment, then the ODE flow expansion at each time instant can be obtained. Moreover, the maximum order of the polynomial expansion for this method is set to $N = 2$. Indeed, this number should be enough to capture the incipient nonlinearity during propagation while not being too computationally demanding. After integration of these equations, a DA polynomial map for the final state will therefore be available up to second order. By truncating this polynomial expansion to first order the state transition matrix up to a certain time step t_k (i.e., $\boldsymbol{\Phi}(t_k)$) is retrieved and the noiseless covariance can be propagated by adopting the LinCov technique [11] as in Eqs. (4 – 6):

$$\mathcal{T}^1_{\mathbf{x}_k}(\boldsymbol{\delta}\mathbf{x}_0) = \boldsymbol{\Phi}(t_k) \tag{4}$$

$$\hat{\mathbf{x}}_k = \boldsymbol{\Phi}(t_k)\mathbf{x}_0 \tag{5}$$

$$\hat{\mathbf{P}}_k = \boldsymbol{\Phi}(t_k)\mathbf{P}_0\boldsymbol{\Phi}^\top(t_k) \tag{6}$$

with the superscript 1 indicating the truncation order of the polynomial map, whereas the accent $\hat{}$ has been used to characterize means and covariances obtained with a linear propagation. On the other hand, the second-order propagation [19] leverages the Isserlis' formula with maximum order $N = 2$, and is instead indicated with the $\tilde{}$ accent $\tilde{\mathbf{x}}_k$ and $\tilde{\mathbf{P}}_k$. The two distributions are compared at t_k according to the Hellinger Distance H to determine the need to split the current Gaussian distribution [28], which expresses the distance between the two distributions and can therefore inform about the onset of nonlinearity during propagation. Moreover, it has the interesting property of being bounded between 0 and 1, which allows setting nonlinearity thresholds that should hold true for varying test cases.
ADAGMM is further adapted to account for the covariance inflation term owed to the presence of thrust noise. This is done as a one step correction of the covariance when the GME reaches its final propagation time. The computation of this inflation term from the initial time of the propagation t_0 until the final time t_f can be obtained

as [12]:

$$\mathbf{\Delta P} = \int_{t_0}^{t_f} \mathbf{\Phi}(\tau)\mathbf{G}(\tau)\mathbf{Q}\mathbf{G}^\top(\tau)\mathbf{\Phi}^\top(\tau)d\tau \qquad (7)$$

In this equation the term $\mathbf{Q}$ is adopted to describe the covariance of the process noise $\mathbf{w}$. The state transition matrix $\mathbf{\Phi}(\tau)$ is retrieved automatically from the DA expansion of the flow. Similarly, $\mathbf{G}(\tau)$ is given by the gradient of the dynamics with respect to the input perturbation $\mathbf{G}$ evaluated about the nominal trajectory. If the Hellinger distance threshold is violated, the propagation of the GME is stopped, the GME is split in a GMM, and each of the new components is corrected for covariance inflation from the beginning of their propagation up to the achieved splitting instant. The direction in which the GME has to be split is determined thanks to the a state-of-the-art algorithm presented in [29]. By knowing the number of desired splits n_s, a univariate splitting library [23] is applied in the desired direction. The outcome of this sub-routine is a new set of new means, covariances, and weights at the initial time of the propagation t_0 for the current GME that needed splitting. Thanks to the polynomial map $[\mathbf{x}_*](\boldsymbol{\delta}\mathbf{x}_0)$ it is possible to propagate each of the newly generated GMEs directly up to the splitting time without having to integrate each one of them numerically. The newly expanded maps can be used with the Isserlis' formula to retrieve the propagated means and covariances. Moreover, these new expansions can also be exploited in Eq. (7) to compute the covariance inflation terms appropriately for each of the new GMEs going from t_0 to the splitting time. At the end of the split procedure, the new set of GMEs at their new initial time is added to the list of GMEs that need to be propagated and their starting time is set to be t_0 for the next propagation. The total number of GMEs cumulated during the automatic split procedure will grow exponentially with the number of splits, hence, the computational effort can be limited by bounded by tuning the number of GMEs for each split and the split threshold.

2.3. Stochastic Taylor Model

The second method proposed extends DA to include the possibility of handling process noise in uncertainty propagation. The key idea of the STM approach is to obtain a polynomial expansion of the ODE flow for the state which is endowed with a linearized correction term for the covariance to account for the thrust noise. The overall procedure can be summed up as a sequence of steps:

1. The initial state is set as a DA variable and its ODEs are propagated to retrieve an higher-order expansion of the flow with respect to the initial state variation. This system of ODEs is coupled with additional equations accounting for the linearized correction of the covariance. This coupling allows to retrieve the covariance inflation term as an expansion of the initial condition, therefore it can be used to re-expand this correction term about any trajectory stemming from an initial condition in the neighborhood of the initial state.
2. After propagating these two polynomial maps a DA Monte Carlo simulation is performed on the state map to retrieve the final distribution of states.
3. A GMM is then fit to this point cloud so that a set of means, weights, and covariances can be used to describe the final distribution.
4. The initial state that generates each mean of the final GMM is obtained through a polynomial map inversion of the ODE flow of the state.
5. Then, these initial conditions can be used to evaluate the polynomial map of the covariance inflation. This term is simply summed to the final covariance of each GME without modifying its weight.

The initial state of the propagation needs to be set as a DA variable and the following set of equations is propagated from the initial conditions $[\mathbf{x}_0] = \mathbf{x}_0 + \boldsymbol{\delta}\mathbf{x}_0$ and $\mathbf{\Delta P}_0 = \mathbf{0}$:

$$\dot{\mathbf{x}} = \mathbf{f}\left(t, \mathbf{x}, \mathbf{u}\right) \qquad (8)$$

$$\dot{\mathbf{\Delta P}} = \mathbf{F}\mathbf{\Delta P} + \mathbf{\Delta P}\mathbf{F}^\top + \mathbf{G}\mathbf{Q}\mathbf{G}^\top \qquad (9)$$

Having adopted the notation $\mathbf{G}$ and $\mathbf{F}$ to characterize the partial of the dynamics with respect to the control and state. Through the dependency from these partials, also $\mathbf{\Delta P}$ is retrieved as a polynomial expansion about the initial state. Therefore, at the desired final time of the propagation two polynomial expansions will be available, one for the state such as in Eq. (3) and one for the covariance inflation:

$$[\mathbf{\Delta P}_f] = \mathbf{\Delta P}_f + \mathcal{T}_{\mathbf{\Delta P}_f}(\boldsymbol{\delta}\mathbf{x}_0) \qquad (10)$$

The reasoning behind this approach is to propagate only the covariance inflation term owed to the presence of thrust noise in the region neighbouring the nominal trajectory. By adopting a polynomial expansion of the ODE flow, it becomes possible to re-expand the covariance inflation term about any trajectory sampled from the state transition map. Eq. (9) can be retrieved according to the following procedure that relies on propagating covariance with and without process noise [12]:

$$\dot{\overline{\mathbf{P}}} = \mathbf{F}\overline{\mathbf{P}} + \overline{\mathbf{P}}\mathbf{F}^\top + \mathbf{G}\mathbf{Q}\mathbf{G}^\top \qquad (11)$$

$$\dot{\mathbf{P}} = \mathbf{F}\mathbf{P} + \mathbf{P}\mathbf{F}^\top \qquad (12)$$

By making the assumptions of local linearization[12], the presence of thrust noise does not influence the nominal trajectory. As a consequence $\mathbf{F}$ and $\mathbf{G}$ will be the same for both set of ODEs. These assumptions imply that the bulk of nonlinearity in the uncertainty propagation will depend on the unperturbed nonlinear motion and will be captured by the high-order expansion of the flow of ODEs for the mean. On the other hand, they also entail that the process noise will be account for a term that can be

obtained via local linearization and that does not significantly impact the propagation of the mean state.

The realization of the final state ODE flow expansion allows to exploit the DA Monte Carlo approach to propagate a large number of samples drawn from the initial distribution and propagated through the polynomial map [19, 30]:

$$\mathbf{x}_f^n = \mathbf{x}_f + \mathcal{T}_{\mathbf{x}_f}\left(\mathbf{x}_0^n - \mathbf{x}_0\right) \tag{13}$$

with $\mathbf{x}_0^n$ and $\mathbf{x}_f^n$ being the initial and final state of the n-th sample.
This procedure produces a point cloud at t_f, which can be fitted with an arbitrary n_s number of GME elements. Each GME has a specific mean $\mathbf{x}_f^s$, covariance $\mathbf{P}_f^s$ and weight w_f^s. The higher the weight, the more the linked GME contributes to the Probability Density Function (PDF) at t_f. Up to this point, the GMEs do not take into account thrust noise covariance. To include this contribution, the polynomial map is exploited a second time. In particular, by exploiting polynomial map inversion and evaluating it for each mean of the final GME

$$\boldsymbol{\delta}\mathbf{x}_0^s = \mathcal{T}_{\mathbf{x}_f}^{-1}\left(\mathbf{x}_f^s - \mathbf{x}_f\right) \tag{14}$$

it becomes possible to retrieve the variation from the initial condition that generated the mean of the current GME under investigation. This initial variation can be used in the evaluation of the covariance inflation term for each mean of the GME by evaluating Eq. (10). Once $\boldsymbol{\Delta}\mathbf{P}_f^s$ has been evaluated for every GME, the covariance inflation term is simply summed to the final covariance of the mixand $\mathbf{P}_f^s$.

3. PROBABILISTIC BASED UNCERTAINTY PROPAGATION

3.1. Dynamical Stochastic Model of Maneuvering Objects

Let us consider the dynamics of a manoeuvring spacecraft. The nominal acceleration generated by the thruster at time t is denoted $\mathbf{a}_T(t)$ and, if we assume that this magnitude is deterministic and exact, then the dynamics of the orbiting spacecraft is given by the ODE

$$\dot{\mathbf{v}} = -\mu\frac{\mathbf{r}}{r^3} + \frac{1}{2}\rho_r v_{rel} B\mathbf{v}_{rel} + \sum_l \mathbf{p}_{J_l} + \mathbf{a}_T(t)$$

where $\sum_l \mathbf{p}_{J_l}$ is the superposition of perturbations due to the zonal harmonics. In a practical setup, however, the thruster acceleration is subject to unknown perturbations. We model this uncertainty by transforming the ODE above into the stochastic differential equation (SDE) in Itô form [31]

$$\mathrm{d}\mathbf{r} = \mathbf{v}t\,, \qquad \mathrm{d}\mathbf{v} = \mathbf{f}(\mathbf{X},t)\mathrm{d}t + \mathbf{G}(\mathbf{a}_T)\mathrm{d}\mathbf{W} \tag{15}$$

where $\mathbf{X}(t) = [\mathbf{r}(t)^\top, \mathbf{v}(t)^\top]^\top$,

$$\mathbf{f}(\mathbf{X},t) = -\mu\frac{\mathbf{r}}{r^3} + \frac{1}{2}\rho_r v_{rel} B\mathbf{v}_{rel} + \sum_l \mathbf{p}_{J_l} + \mathbf{a}_T(t)\,, \tag{16}$$

is a drift function representing the deterministic part of the dynamics, $\mathbf{W}(t)$ is a standard 3-dimensional Wiener process (Brownian motion) with diffusion coefficient $\mathbf{G}(\mathbf{a}_T)$. The term $\mathbf{G}(\mathbf{a}_T)\mathrm{d}\mathbf{W}$ is a stochastic diffusion that accounts for the uncertainty in the acceleration generated by the thruster. The matrix $\mathbf{G}(\mathbf{a}_T)$ controls the power of the acceleration 'noise'. When $\mathbf{G}(\mathbf{a}_T)$ depends on the nominal thruster acceleration but not on the state of the spacecraft, the Itô equation (15) matches the Stratonovich SDE [31] (see also Chapter 6 of [32]). Since the state of the spacecraft is the 6-dimensional vector $\mathbf{X}(t)$, we find it more convenient to rewrite (15) in the more compact form

$$\mathrm{d}\mathbf{X} = \tilde{\mathbf{f}}(\mathbf{X},t)\mathrm{d}t + \tilde{\mathbf{G}}(\mathbf{a}_T)\mathrm{d}\mathbf{W}, \tag{17}$$

where $\tilde{\mathbf{f}}(\mathbf{X},t) = \begin{bmatrix}\mathbf{v}(t)\\ \mathbf{f}(\mathbf{X},t)\end{bmatrix}$ and $\tilde{\mathbf{G}}(\mathbf{a}_T) = \begin{bmatrix}\mathbf{0}_{3x3}\\ \mathbf{G}(\mathbf{a}_T)\end{bmatrix}$.

If the last term in is neglected (i.e., we set the covariance matrix $\mathbf{G}(\mathbf{a}_T) = 0$ for all t), the dynamics become deterministic.

Choices for the diffusion coefficient $\mathbf{G}(\mathbf{a}_T)$ We assume the nominal acceleration $\mathbf{a}_T$ is known for all t. One key issue that will be important later for the design of numerical schemes is whether $\mathbf{a}_T$ depends on $\mathbf{X}(t)$ or not. For the case described below, a physical model for $\mathbf{G}$ has been developed with an explicit dependence on $\mathbf{X}(t)$.

Let us denote the true acceleration generated by the thruster as $\mathbf{a}_T^* = a_T^*\tau^*$ where $a_T = ||\mathbf{a}_T^*||$ and τ^* is the unit vector in the direction of the acceleration. The latter can be written as a function of the unit vectors $\mathbf{i}\,,\mathbf{j}\,,\mathbf{k}$ along the spatial directions as:

$$\tau^*(\alpha,\beta) = \cos\alpha\cos\beta\mathbf{i} + \sin\alpha\sin\beta\mathbf{j} + \sin\beta\mathbf{k} \tag{18}$$

where the angles α and β hence determine the direction of the thrust. Then, we may have two physical sources of uncertainty: the thrust produced by the propulsion system (a_T^*) and the pointing of the spacecraft ($\tau^*(\alpha,\beta)$). If we let a_T denote the reference or nominal value magnitude of the acceleration and also assume known reference values for the pointing, denoted $\alpha_r;\beta_r$, the difference of the actual and nominal values can be characterised as Gaussian errors:

$$\Delta a_T = a_T^* - a_T \sim \mathcal{N}(m_{\Delta,a}, \sigma_{\Delta,a}^2)\,, \tag{19}$$

$$\Delta\mathbf{y} = \{\Delta\alpha, \Delta\beta\}^T \sim \mathcal{N}(\mathbf{m}_{\Delta,y}, \boldsymbol{\Sigma}_\Delta)\,, \tag{20}$$

With this notation, we may write the true acceleration $\mathbf{a}_T$ as:

$$\mathbf{a}_T^* = (a_T + \Delta a_T)\tau^*(\alpha_r + \Delta\alpha, \beta_r + \Delta\beta) \tag{21}$$

If we assume $\Delta\alpha \ll 1$ and $\Delta\beta \ll 1$, then $\cos\Delta\alpha \sim 1 \sim \cos\Delta\beta$, $\sin\Delta\alpha \sim \Delta\alpha$, $\sin\Delta\beta \sim \Delta\beta$ and $\Delta\alpha\Delta\beta \ll 1$. Thus, we write the direction vector as $\tau^* = \tau_r + \Delta\tau$, with:

$$\begin{aligned} \tau_r &= \cos\alpha_r \cos\beta_r \mathbf{i} + \sin\alpha_r \sin\beta_r \mathbf{j} + \sin\beta_r \mathbf{k}\,, \\ \Delta\tau &= \mathbf{S}\Delta\mathbf{y}\,, \end{aligned}$$

and,

$$\mathbf{S} = \begin{bmatrix} -\cos\beta_r \sin\alpha_r & \cos\alpha_r \sin\beta_r \\ \cos\alpha_r \cos\beta_r & -\sin\alpha_r \sin\beta_r \\ 0 & \cos\beta_r \end{bmatrix}.$$

Finally, the acceleration generated by the thruster can be written as

$$\mathbf{a}_T^* = a_T\tau_r + \mathbf{a}_T^{(1)} + \mathbf{a}_T^{(2)}\,,$$

where $\mathbf{a}_T^{(1)}, \mathbf{a}_T^{(2)}$ are random, with

$$\begin{aligned} \mathbf{a}_T^{(1)} &= \Delta a_T \tau_r \sim \mathcal{N}(m_{\Delta,a}\tau_r, \sigma^2_{\Delta a_T}\tau_r\tau_r^T) \\ \mathbf{a}_T^{(2)} &= a_T\mathbf{S}\Delta\mathbf{y} \sim \mathcal{N}(a_T\mathbf{S}\mathbf{m}_{\Delta,y}, a_T^2\mathbf{S}\boldsymbol{\Sigma}_\Delta\mathbf{S}^T) \end{aligned}$$

Recalling (16), we can now write the drift function $\mathbf{f}(\mathbf{X}, t)$ as

$$\mathbf{f}(\mathbf{X},t) = -\mu\frac{\mathbf{r}}{r^3} + \frac{1}{2}\rho_r v_{rel} B\mathbf{v}_{rel} + \sum_l \mathbf{p}_{J_l} + ... \\ + a_T\tau_r + m_{\Delta,a}\tau_r + a_T\mathbf{S}\mathbf{m}_{\Delta,y}\,, \quad (22)$$

and the diffusion coefficient as $\mathbf{G}(\mathbf{a}_T) = \begin{bmatrix}\sigma_{\Delta a_T}\tau_r & a_T\mathbf{S}\sqrt{\boldsymbol{\Sigma}_\Delta}\end{bmatrix}$. This diffusion model implies that process $\mathbf{G}(\mathbf{a}_T)\mathrm{d}\mathbf{W}$ has a covariance matrix

$$\mathbf{R}(\mathbf{a}_T) = h\mathbf{G}(\mathbf{a}_T)\mathbf{G}^\top(\mathbf{a}_T) = h\sigma^2_{\Delta a_T}\tau_r\tau_r^\top + ha_T^2\mathbf{S}\boldsymbol{\Sigma}_\Delta\mathbf{S}^\top \quad (23)$$

over intervals of length $h \ll 1$.

Numerical Schemes There are variety of numerical schemes that can be employed to approximate the Itô process described by Eq. (15). The numerical schemes implemeted for this work were a 1.0 order stochastic Runge-Kutta (SRK) method from [33] with *strong convergence* [34], and a *weak* order 3.0 SRK scheme from [35], which is more complex but enjoys better theoretical properties.

3.2. Uncertainty Propagation Methods

The uncertainty on the state of an orbiting object is typically represented by an expected or mean value (of both position and velocity in 3-dimensional space) together with a covariance matrix that accounts for the expected error with respect to the mean. As Gaussian distributions are fully determined by its two first moments, it is just natural to interpret this uncertainty characterization as a normal distribution on the state at time 0, i.e., $\mathbf{x}_0 \sim \mathcal{N}(\bar{\mathbf{x}}_0, \mathbf{C}_0)$, where $\bar{\mathbf{x}}_0$ and $\mathbf{C}_0$ are the mean and covariance, respectively, at time 0.

Let $p_n(\mathbf{x}_n)$ denote the PDF of the state $\mathbf{x}_n$ of the orbiting object at time $t = nh$. Gaussian methods for UP construct a normal approximation of $p_n(\cdot)$ by propagating the initial mean $\bar{\mathbf{x}}_0$ and covariance $\mathbf{C}_0$ to time n using the dynamical equation $\mathbf{x}_n = \Phi_n(\mathbf{x}_{n-1}, \mathbf{u}_n)$. Thus, we approximate $p_n(\mathbf{x}_n) \approx \mathcal{N}(\mathbf{x}_n|\bar{\mathbf{x}}_n, \mathbf{C}_n)$, where $\bar{\mathbf{x}}_n$ and $\mathbf{C}_n$ are the estimated mean and covariance at time n.

There are different ways in which the propagation of the mean state and its covariance can be implemented. The most straightforward solution is the linearisation of the dynamical equation, typically using a first order Taylor approximation [36, 37, 38, 39] or by statistical linearisation [40]. These approaches, however, are known to yield poor results depending on the geometry of the orbit or the length of the propagation period. Instead of linearising the dynamics, a more efficient approach is to estimate the mean and covariance transformed by the nonlinear dynamic equation. Here we review few of the most popular approaches.

Unscented Transform. The UT provides an efficient procedure to propagate both the mean and the covariance through a nonlinear function using deterministic samples. If the mean and covariance before the nonlinear transformation are exact, then the estimates obtained via the UT are accurate up to the second order of a Taylor expansion [41]. Algorithms that rely on the UT can be computationally fast, however they are only useful when the target probability distribution can be 'well approximated by a Gaussian. This precludes multimodal, heavy-tailed and/or asymmetric distributions. For orbital UP, the PDF of the state eventually becomes strongly non-Gaussian (see, e.g., Fig. 2 in [42]). However, the normal approximation can remain useful and rather accurate for short-to-midterm UP, depending on the type of orbit and the relevant perturbations [43]. Other Gaussian UP methods based on deterministic sampling and integration can be designed using cubature theory [44, 45] and they are discussed in next sub-section. Let $\bar{\mathbf{x}}_0$ and $\mathbf{C}_0$ be the mean and covariance at time 0. To apply the UT, we select a set of sigma-points $\mathbf{x}_0(i)$ band associated weights $w_0(i), i = 1, \ldots, 2d+1$, where d is the dimension of $\mathbf{x}_0$. There are many ways in which both the $\mathbf{x}(i)$'s and the $w_0(i)$'s can be computed from $\bar{\mathbf{x}}_0$ (see [46] for an extensive survey) and the number of points, their location and their weights may vary. For example, if a Gauss-Hermite quadrature rule is used, a larger number of points is needed but the approximations are more accurate as well. In any case, the weighted sigma-points should capture the mean and covariance of the initial state exactly. In a second step, the sigma-points are mapped through the non-linear dynamical equation. Let us assume a deterministic scheme $\mathbf{x}_n = \Phi_n(\mathbf{x}_{n-1}, \mathbf{0})$ and denote the composition of n successive steps as

$$\Phi_{0:n} = \Phi_n \circ \Phi_{n-1} \circ \cdots \circ \Phi_1\,,$$

then, the new sigma-points at times n are

$$\mathbf{x}_n(i) = \Phi_{0:n}\left(\mathbf{x}_0(i)\right), i = 1, \ldots, 2d+1,$$

while the weights remain unchanged, $w_n(i) = w_0(i)$. Then the approximate mean at time n is $\bar{\mathbf{x}}_n = \sum_i w_n(i)\mathbf{x}_n(i)$ and the covariance is $\mathbf{C}_n = \sum_i w_n(i)\left(\mathbf{x}_n(i) - \bar{\mathbf{x}}_n\right)\left(\mathbf{x}_n(i) - \bar{\mathbf{x}}_n\right)^\top$. Let us note that the UT can be applied without computing any derivatives. A linearisation of the model is implicit, though (i.e., the UT can be re-written as a linearisation method under certain assumptions). UT algorithms are simple to implement, however their performance may vary depending, e.g., on the number of sigma-points or the type of nonlinearity.

Unscented Kalman filters. In some scenarios, the propagation of uncertainty involves the assimilation of available data. In such cases, the problem is not one of pure prediction anymore but the estimates of the mean $\bar{\mathbf{x}}_n$ and the covariance $\mathbf{C}_n$ have to be updated when relevant data are received. Since the early 2000s, the UT has become a favourite tool for the implementation of (approximate) nonlinear Kalman filters [41, 47] and there is currently a broad choice of so-called unscented Kalman filters (UKFs) tailored to various assumptions [46]. In recent years new versions of the UKF have appeared that have shown behaviors similar to those of the classic UKF but with an even lower computational cost than this. The authors of [48] offer a comparison between different nonlinear filters, including two based on the UKF: single propagation UKF (SPUKF) and extrapolated single Propagation UKF (ESPUKF). The results with cubeSats show that the latter reduce the computational cost by almost half while maintaining the accuracy of the UKF. Filtering methods have also been applied to satellite problems with orbit modification. Thus, [49] apply UT for the design of the trajectory of satellites with reduced impulse (low thrust) in the context of stochastic dynamics. Applications to the determination or transfer of orbit in low thrust regime can be found, also in [49, 50, 51, 52].

Cubature Methods. The term "cubature" refers to a class of methods for the numerical approximation of high-dimensional integrals, i.e., generalizations of classical quadrature schemes to multidimensional settings. The use of cubature methods for uncertainty quantification and filtering gained attention in the engineering community after the publication of [53]. In the framework of UP, the cubature methods are applied in a way that is very similar to UT schemes. The key element is the identification of a set of reference (or cubature) points in the state space and their propagation through a nonlinearity in order to approximate integrals of nonlinear transformations of Gaussian random variables. The key feature of cubature schemes is that they are designed to be exact for a certain class of nonlinear transformations. The practical use of cubature schemes for numerical integration depends on a trade-off between accuracy and computational cost. From this perspective, spherical-radial cubature rules are particularly popular [44, 45]. The spherical-radial cubature rule of the third-degree (SRC3D) [44] is very similar to the UT. Given an initial mean vector $\bar{\mathbf{x}}_0$ and a covariance matrix $\mathbf{C}_0 = \mathbf{S}_0\mathbf{S}_0^\top$, one computes the cubature points

$$\mathbf{x}_0(i) = \sqrt{d}\mathbf{e}^i$$

,

$$\mathbf{x}_0(i+d) = -\sqrt{d}\mathbf{e}^i$$

. For $i = 1, \ldots, d$ and $\mathbf{e}^i$ a vector of 0's with a single 1 in the i-th entry. The weights for these cubature points are all equal, $w_0(i) = w_0 = \frac{1}{2d}$ for $i = 1, \ldots, 2d$. With this choice of cubature points, one can guarantee the identity $\int g(\mathbf{x})\mathcal{N}(\mathbf{x}|\bar{\mathbf{x}}_0, \mathbf{C}_0)\mathrm{d}\mathbf{x} = \sum_i g(\mathbf{x}_0(i))w_0$ when $g(\mathbf{x})$ is a polynomial of degree 3 or less. If we want to propagate the Gaussian distribution of $\mathbf{x}_0$ up to time n through a dynamical equation $\mathbf{x}_n = \Phi_{0:n}(\mathbf{x}_0)$ we simply project the cubature points, $\mathbf{x}_n(i) = \Phi_{0:n}(\mathbf{x}_0(i)), i = 1, \ldots, 2d$, and keep the uniform weight $w_n = w_0 = \frac{1}{2d}$. Then, for a test function $g(\cdot)$, we approximate $\int g(\mathbf{x})p_n(\mathbf{x}_n)\mathrm{d}\mathbf{x}_n \approx \sum_i g(\mathbf{x}_n(i))w_n$. We note that even if the test function $g(\cdot)$ is a polynomial of suitable degree (≤ 3) the cubature estimate is not exactly anymore because $p_n(\mathbf{x}_n)$ is not Gaussian when $\Phi_{0:n}$ is nonlinear. Cubature rules can be obtained for higher order polynomials; see, e.g., rules for polynomials of degree 5 in [44] and [45] (with $\mathcal{O}(d^2)$ cubature points) and rules for polynomials up to degree 7 in [54] (with $\mathcal{O}(d^3)$ cubature points).

Kernel Density Estimators. A natural extension of Gaussian UP methods is to approximate the PDF of the state $p_n(\mathbf{x}_n)$ as a mixture of N normal distributions [55], i.e., $p_n(\mathbf{x}_n) \approx \hat{p}_n^N(\mathbf{x}_n)\sum_{i=1}^N \mathcal{N}(\mathbf{x}_n|\hat{\mathbf{x}}_n^i, b^2\mathbf{\Sigma})$, where the $\mathbf{x}_n^i$'s are the means of the Gaussian kernels, $\mathbf{\Sigma}$ is a covariance matrix and b is a bandwidth parameter. While Gaussian mixture models (GMM) with an adaptive number of components (N) have become popular (see Section 6.x), here we restrict our attention to GMMs with fixed N. In this case, the UP process consists in creating an initial kernel density estimator (KDE),

$$p_0(\mathbf{x}_0 \approx \sum_{i=1}^N \mathcal{N}(\mathbf{x}_0|\hat{\mathbf{x}}_0^i, b^2\mathbf{\Sigma})$$

, and then propagating the N mixands over time using UT or cubature methods. Classical theory on KDEs [56, 57] can be used to prove that, provided the initial means $\hat{\mathbf{x}}_0^i, i = 1, \ldots, N$, are iid samples from $p_0(\mathbf{x}_0)$ and some mild regularity assumptions are met, then the asymptotic convergence of the mean integrated square error (MISE) is guaranteed, i.e.,

$$\lim_{N\to\infty} \mathbb{E}\left[\int \left(p_n(\mathbf{x}) - \hat{p}_n^N(\mathbf{x})\right)^2 \mathrm{d}\mathbf{x}\right] = 0$$

. If $p_n(\cdot)$ is Lipschitz, then [58] provides stronger results. In particular,

$$\sup_{\mathbf{x}} |p_n(\mathbf{x}) - \hat{p}_n^N(\mathbf{x})| \leq \frac{V_\epsilon}{N^{\frac{1-\epsilon}{2(d+1)}}}$$

, where $\epsilon > 0$ is arbitrarily small, V_ϵ is an a.s. finite random variable and $b = \mathcal{O}\left(N^{\frac{-1}{2(d+1)}}\right)$. While these results provide guarantees for large N, in a practical orbital UP application the number of mixands N in the GMM should be at most moderate. In this case, the key to the performance of the estimator is the choice of the bandwidth parameter b. However, $\hat{p}_n^N(\cdot)$ often displays artifacts in the tails of the distribution. Work is usually needed to design bandwidth selection schemes that avoid this (undesired) feature.

4. NUMERICAL SIMULATIONS

This section provides a description of the analyzed test cases. For the proposed methods, the dynamics of the systems are assumed to be defined by:

$$\begin{aligned}\dot{\mathbf{x}} &= \mathbf{f}(t, \mathbf{x}, \mathbf{u} + \mathbf{w}) = \\ &= \begin{cases} \dot{\mathbf{r}} = \mathbf{v} \\ \dot{\mathbf{v}} = -\frac{\mu}{r^3}\mathbf{r} + \frac{1}{2}\rho(r)\left(\frac{C_d A}{m}\right) v^2 + \mathbf{u} + \mathbf{w} \end{cases}\end{aligned} \tag{24}$$

The state is here represented by position and velocity $\mathbf{x} = [\mathbf{r}; \mathbf{v}]$, and it is further assumed that any given control history can be parametrized with a function of time $\mathbf{u}$ plus additive process noise $\mathbf{w}$. In this work the dynamics is assumed to be constituted by Keplerian acceleration with gravitational parameter μ, a simplified drag model, and the thruster acceleration (with its noise). Concerning the drag model, the ballistic coefficient is given by the ratio of front area A times the drag coefficient C_d and it is divided by the mass of the object m. To conclude, the atmospheric density ρ is assumed to be a function of the altitude only. The implemented atmospheric density model needs to cover altitudes of at least 1300 km to provide drag values for all envisioned test cases in LEO. The implemented simplified model relies on the Jacchia77 empirical model [59], which provides density profiles up to 2500 km. To simplify this estimate by reducing it to only a dependence on altitude, the distribution of densities is averaged at different altitudes levels.

The physical model of the thrust noise covariance has been described in the previous section (3), and accordingly, it is assumed that this can be modelled as a pointing and amplitude error. For the envisioned test cases, 4 different combination of increasing uncertainties are adopted and their values are reported in Table 1.

Table 1. Summary of noise levels.

Noise Level	Amplitude error [%]	Angular error [deg]
Accurate	0.5	1.0
Average	1.0	2.0
Low	2.5	5.0
Inaccurate	5.0	10.0

4.1. Test Cases Description

The test cases have been provided with the collaboration of GMV. they include significant scenarios for long-thrusting (e.g., Orbit Raising) and orbit maintenance. Among the operational scenarios involving long thrusting, at least the following ones are considered:

- Low-LEO-to-LEO electric orbit raising, as currently carried out for instance by One-web satellites from around 500 km to around 1200 km following a spiral-like trajectory lasting months.
- GTO-to-GEO electric orbit raising, as currently carried out by GEO satellites equipped with low-thrust devices in order to raise the satellite from GTO orbit to the final GEO orbit.
- LEO disposal, where a LEO satellite orbit is lowered with low-thrust means at its end-of-life in order to comply with the guideline of 25 years maximum orbital lifetime.
- LEO Station Keeping (SK), as currently done by various types of satellites (communications, Earth-observation, etc.) following different strategies (ground-track control, constellation control).
- GEO orbit maintenance, where GEO satellites with electric propulsion carry out daily low-thrust manoeuvres to compensate the orbital disturbances caused by Sun and Moon and the Earth geopotential.

For each of these scenarios, a reference orbit is generated, considering the typical constraints affecting low-thrust devices (e.g. eclipses, maximum slew rates, etc.). These reference orbits are then used to simulate an operational-like situation where measurements are available from the sensors being used, through the simulation of the observations and the subsequent orbit determination process, throughout different phases of the reference orbit. This allows to generate realistic orbital states and covariances, at the time of the last observation. The following sensor networks are considered for the observation simulation process, together with the expected visibility windows:

- On-board GNSS receivers, both below and above GNSS altitude, considering the typical size of primary and secondary lobes of the GNSS signal.
- Ranging stations, used to measure the slant range of the satellite with respect to a network of stations, whose number depends on the orbital regime considered (e.g. two in GEO).
- Space surveillance networks, composed of survey and tracking radars (typically for LEO) and telescopes (typically for MEO and GEO).

The a-posteriori realistic covariances are then used as input to perform the uncertainty propagation using the different approaches to be compared, including the uncertainty of the low-thrust propulsion system. A summary of the study cases is reported in Table 2.

Additionally, in order to assess the suitability of the selected approach for characterizing conjunctions, collisions are also simulated as part of this process with the estimated orbits of the operational satellites (i.e. primary object) and a background population of space debris objects. The simulated conjunctions are reported in Table 3.

5. RESULTS

The accuracy of each scenario will be compared against a Monte Carlo simulation of 50000 samples, the metrics adopted will be:

- Runtime normalized with respect to benchmark MC (500 samples)
- L_2 norm of final mean position and velocity errors
- L_2 norm (i.e., Frobenius norm) of final position and velocity covariance errors
- Maximum Total Variation Distance (TVD) among all states
- Maximum Mean Integrated Square Error (MISE) among all states

These two latter measures have been introduced to account for the non-Gaussianity of the distribution. First, the MISE will be evaluated per each dimension and normalized with the distribution obtained for each dimension by the Monte Carlo analysis. Secondly, also the TVD will be analysed per each dimension. To conclude, only the maximum MISE and maximum TVD will be provided. While these latter metrics should provide some insight into the description of the non-Gaussianity, they only tell part of the story. Indeed, by considering each dimension on its own, all information related to the coupling between variables is lost. When looking at the computational time, each of the reported times have been normalized with the runtime of the corresponding Monte Carlo simulation of 500 samples to reduce the computational effort.

5.1. Comparison of Uncertainty Propagation Approaches

All propagation strategies analyzed showed degrading performances for increasing duration of the propagation across all metrics. To account for this behaviour, while also considering the varying level of thruster error in Table 1, a cumulative index called Process Noise Index (PNI) is used to compare performances of different scenarios and algorithms. This PNI is computed as the ratio between initial and final sizes of the state covariances obtained from the benchmark MC analysis.

$$\text{PNI} = \frac{\det\left(\mathbf{P}_f\right)}{\det\left(\mathbf{P}_0\right)} \tag{25}$$

The results are reported in a series of summary graphs considering all combination of scenarios (i.e., with different markers) and algorithm (i.e., with different colors) when propagated at their final time as reported in Table 2. Each of these combinations will have a 4 different levels of PNI which are determined by the thruster noise performance.
A preliminary look at computational times (e.g., reportd in Figure 1 for dynamics-based methods) reveals that that STM is more costly in terms of computational time, being it on average ~ 0.7. However, its cost is not dependent on the PNI. On the contrary, ADAGMM shows a dependency of the computational time with PNI which is particularly relevant for some scenarios (e.g., LEO to LEO and LEO DISPOSAL). Despite this, it still is faster with an average time across all PNI and scenarios of ~ 0.1. The increase of time for this method is to be expected for some challenging cases where the increasing nonlinearity makes the number of GMEs (adaptively determined) grow very rapidly (i.e., ~ 1000 GMEs for LEO to LEO). With regards to probabilistic based methods, it was observed that consistently for all scenarios, UT and SRC3D methods are below 10% of the reference time for the MC run, whereas SRC5D is on about 20% and KDE methods in the 50%. In addition, it was not observed a direct dependency between PNI and computational time.

Figure 2 shows the effect of PNI on the error of estimation of the mean for dynamics based methods. Both subfigures shows the same trends, with the estimation not significantly influenced by an increase of PNI. STM clearly outperforms ADAGMM in terms of final mean error. Concerning probabilistic approaches, we observed that errors for low PNI are in the order of hundreds of meters for UT and SRC, but they grow exponentially with PNI with UT algorithms showing a steeper slope than SRC. The maximum mean position error observed for the SRC algorithms is about 10 km. On the other hand, KDE algorithms present a performance which is almost independent on PNI, with errors in the order of the km.

Since dynamics-based methods are basically unchanged in terms of position error but they accumulate a growing error in covariance, also the metrics capturing the non-Gaussian behaviours reflect similar trends in Figure 3. While STM has static hyperparameters, ADAGMM can adapt the number of GMEs autonomously even if the parameters are fixed. This trend is clearly visible in the LEO to LEO and LEO DISPOSAL scenarios where the number of GMEs grow but they allow for a better representation of the uncertainty. It is also worth mentioning

Table 2. Operational scenarios investigated.

Scenario	Orbital Regime	Propagation Time [days]	Notes
LEO to LEO	LEO (500 km)	7	Earth Orbit Raising with continuous thrust
LEO DISPOSAL	Low LEO (Starlink)	7	End of disposal for Starlink-like satellite with continuous thrust
LEO SK	Low LEO (Starlink)	3	Daily along-track short maneuvers
GTO to GEO	GTO	15	Beginning of Orbit Raising (i.e., near GTO) with continuous thrust
GEO SK	GEO	15	Daily maneuvers of long duration

Table 3. Analyzed Conjunctions.

Scenario	Relative Speed (m/s)	Conjunction Angle [deg]	Time to Conjunction [days]
LEO to LEO	1000	90	3
LEO DISPOSAL	15000	179	2
LEO SK	5000	40	4
GTO to GEO	16000	178	4
GEO SK	500	70	5

that the LEO SK has very little variation of the PNI because it has the shorter propagation but also very short and few maneuvers. In this case as well as the GEO ones there is substantially no difference between the two approaches. When looking at probabilistic based methods, the results show that the behaviour of the algorithms has a consistent dependence on the PNI. UT algorithms (i.e., see Figure 4) show small values of maximum TVD for low PNI, but the performance degrades fast with PNI. In addition, reduced UT always outperforms the standard UT. Meanwhile, SRC algorithms (i.e., see Figure 5 perform better with low PNI, but the performance is stable with large values of PNI, and below 0.15. Finally, KDE algorithms (i.e., see Fig. 6) show the best performance for large PNI, but they present a worse behaviour than the other two families at low PNIs. The maximum TVD for low PNIs are in the range $0.1 - 0.2$, whereas it goes to around 0.05 for large PNI values in some scenarios (e.g., LEO orbit raising or GEO to GEO). Their behaviour outperforms the other methods in terms of uncertainty realism for large effects of the process noise. However, on the other end, the maximum TVD is around 0.15 for the LEO SK case (where UT methods have a maximum TVD below 0.02). In addition, "coarse" bandwidth KDE (0.7) presents, in general, a better performance than the "fine" bandwidth. This behaviour seems to change for large PNI values.

5.2. Conjunction Analysis

Five conjunction scenarios described Table 3 have been analysed with the proposed uncertainty propagation methods. Each of the approaches produces two final GMMs to represent the final distributions at the estimated Time of Closest Approach (TCA) for primary and secondary objects. When both GMMs are available, the following method is adopted to compute the PoC[23]:

- Selecting a combination of a GME from the primary's GMM and a GME from the secondary's GMM.
- Searching for the correct TCA of the combination.
- Propagating locally the mean and covariance of both GMEs to the real TCA.
- Computing the PoC of the combination with a short-term encounter model such as Chan's model [60].
- Summing all contributions from all possible combinations of GMEs .

The summary of results is reported in Table 4.

The number of splits for STM and KDE has been selected after a trade-off analysis carried out on all scenarios which lead to the selection of 15 and 20 splits respectively. In addition, the reference linear propagation, UT, RUT, and SRC have always 1 GME for both primary and secondary by definition. On the other hand, ADAGMM determines this number automatically during propagation.
In the GEO SK scenarios nonlinearities are so small that no splits were determined by ADAGMM so that the same results as a local linearization are retrieved. For the same reason, also STM retrieved very small variations of PoC for varying number of GMEs. As Table 2 demonstrates, the PoC obtained with dynamics-based methods is always close to the value obtained through a linear propagation. This behaviour is expected as all the methods presented treat process noise with local linearizations built upon

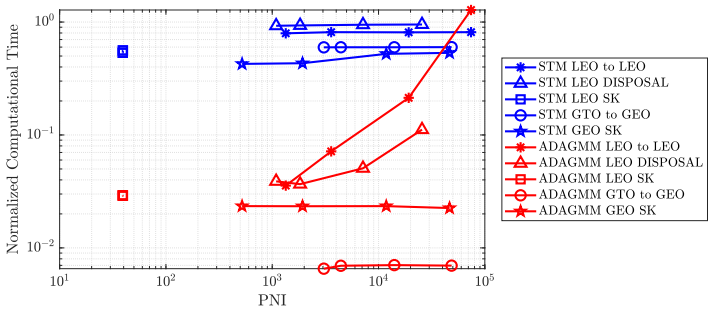

Figure 1. Normalized computational time for all combinations of scenario, method, and thruster uncertainty for dynamics based approaches.

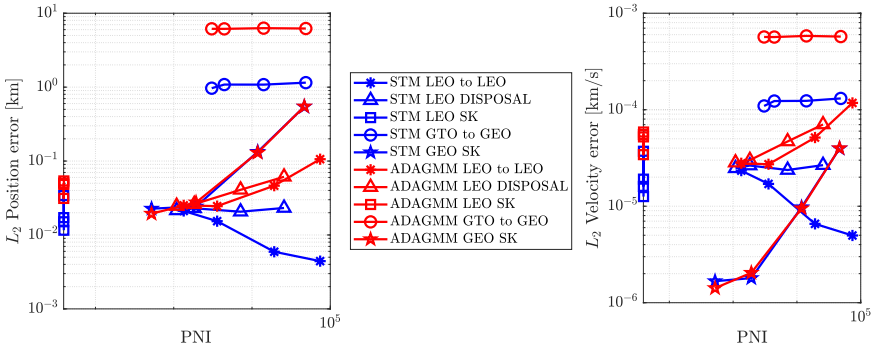

Figure 2. Error in the final mean position (left) and velocity (right) for all combinations of scenario, method, and thruster uncertainty for the dynamics based methods.

higher order information extracted from the flow of the dynamics.

On the contrary, probabilistic-based methods relied on a stochastic propagation which modified the conjunction geometry. As a consequence, the PoC was close to the one obtained by linear propagation for small PNI, whereas it was diluted (even to 0) for higher values of PNI. To validate the approaches, a MC analysis was also carried out for the two bounding cases: GTO to GEO, and GEO SK. For the first case, the number of samples was selected with Dagum's formula [61] in order to have a 95% confidence interval and a 10% relative error. The MC clearly shows that the linear propagation is underestimating the real probability whereas dynamics-based methods are overestimating it. For the second case, the number of samples was determined to have a 95% confidence with a 5% relative error. The results show a PoC that substantially matches that obtained via linear propagation.

6. CONCLUSIONS

Both dynamics-based and probabilistic-based methods retrieve consistent results. For intrusive methods, different ways of including a covariance correction term based on local linearization output similar results. Despite being much faster than a MC analysis, the accuracy of these methods is not always excellent. One hypothesis is that this behavior is to be imputed to the process noise modelling. Indeed, the presented methods seem to miss the effect of the coupling between initial state uncertainty and thruster noise, resulting in an underestimation of the covariance when compared to the results of the MC analysis. Moreover, the mono-dimensional comparison metrics selected (i.e., MISE and TVD) may be penalizing dynamics-based methods that retrieve a full PDF description even considering coupling terms, whose contribution is completely discarded by these criteria.

Concerning probabilistic-based methods, a suite of algorithms has been tested for uncertainty propagation in different orbital and manoeuvre scenarios with different thrust noise levels.

The computational cost, when compared to a MC algorithm used as benchmark, is almost constant and independent on the scenario or the thrust noise level. UT algorithms have the minimum cost (below 10%), SRC show an intermediate performance, while KDE runtime is more than half of the corresponding MC. In terms of computational time DAGMM offer the best performance (on average) in line with UT methods. SRC approaches provide a good middle ground, while KDEs and STM methods seem to be the most computationally expensive techniques.

When comparing accuracy of these approaches in terms of uncertainty realism, one can observe how different families of probabilistic approaches show consis-

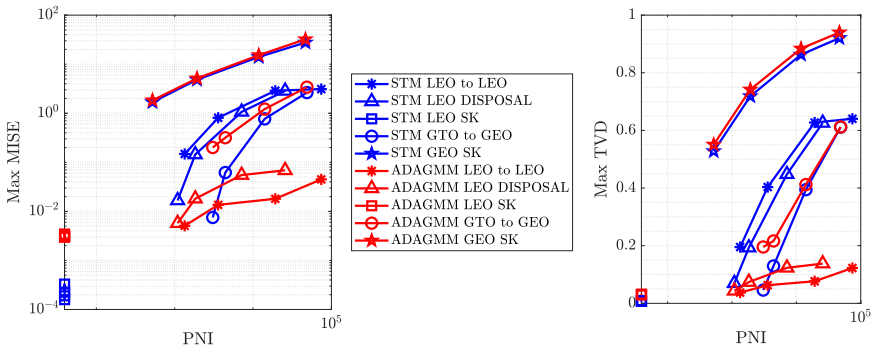

Figure 3. MISE (left) and TVD (right) for all combinations of scenario, method, and thruster uncertainty for dynamics based methods.

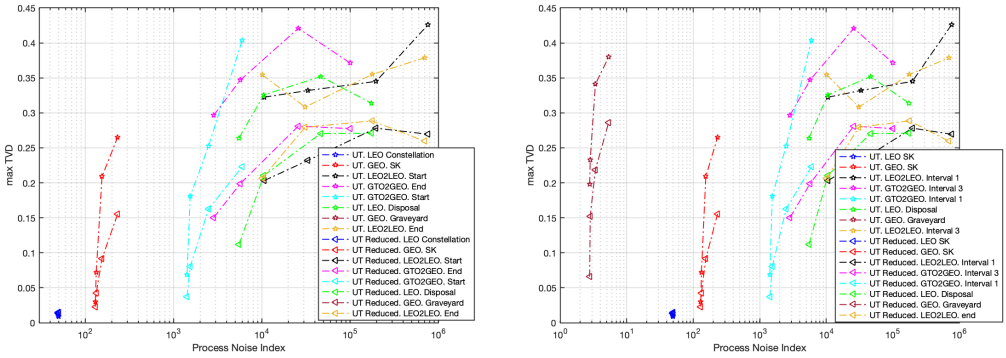

Figure 4. TVD for all combinations of scenario and process noise with UT and reduced UT methods.

tent trends: i.e., UT methods work best for low PNI while KDEs are better suited for propagations where higher uncertainties are involved, whereas SRC methods provide a middle ground between the two. On the contrary, dynamics-based methods show similar performance degradation. Their trend is closer to that of UT, which they also match in terms of the other performance metrics. In addition, discrepancies between dynamics-based methods are mostly related to the different scenario of propagation rather than the level of noise involved.
The maximum TVD provides with the information of the ability of a given algorithm to match the reference probability density function of the spacecraft state. However, due to the uncertainty growth, even low values of the TVD could be high for conjunction assessment. This fact can be seen in the mean position error provided by each probabilistic-based method with respect to the benchmark. Only SRC and UT in a less extent provide mean position errors in the orders of tens of meters in the scenarios with lowest PNI. Although KDE algorithms are able to cope with scenarios with large PNI, the mean position error is in the order of hundreds of meters or kilometre which ends up diluting the PoC computed. On the contrary, dynamics-based methods proved to be effective in capturing the conjunction scenario and the results were always consistent to the reference PoC computed with linearly propagated uncertainties.

7. ACKNOWLEDGMENT

This activity has been carried out under the ESA funded project ELECTROCAM.

REFERENCES

1. K. Holste, P. Dietz, S. Scharmann, K. Keil, T. Henning, D. Zschätzsch, M. Reitemeyer, B. Nauschütt, F. Kiefer, F. Kunze, J. Zorn, C. Heiliger, N. Joshi, U. Probst, R. Thüringer, C. Volkmar, D. Packan, S. Peterschmitt, K. T. Brinkmann, H.-G. Zaunick, M. H. Thoma, M. Kretschmer, H. J. Leiter, S. Schippers, K. Hannemann, and P. J. Klar. Ion thrusters for electric propulsion: Scientific issues developing a niche technology into a game changer. *Review of Scientific Instruments*, 91(6):061101, June 2020.
2. Ben Larbi, M K Grzesik, B Radtke, C J Trentlage, and E Stoll. Active debris removal for mega constellations: Cubesat possible. In *Proceedings of the 9th International Workshop on Satellite Constellations and Formation Flying, IWSCFF2017, 19-21 June, 2017, Boulder, Colorado*, pages 1–19. IAF, 2017. Paper No. IWSCFF 17-20.
3. Javier Hernando-Ayuso and Claudio Bombardelli. Low-Thrust Collision Avoidance in Circular Or-

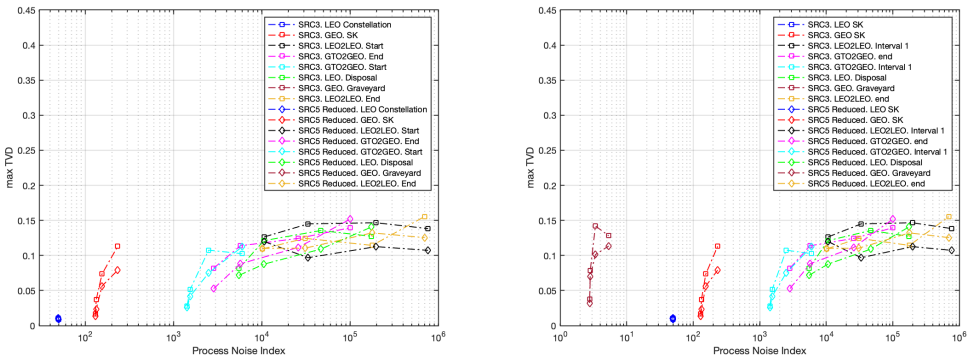

Figure 5. TVD for all combinations of scenario and process noise with SRC methods.

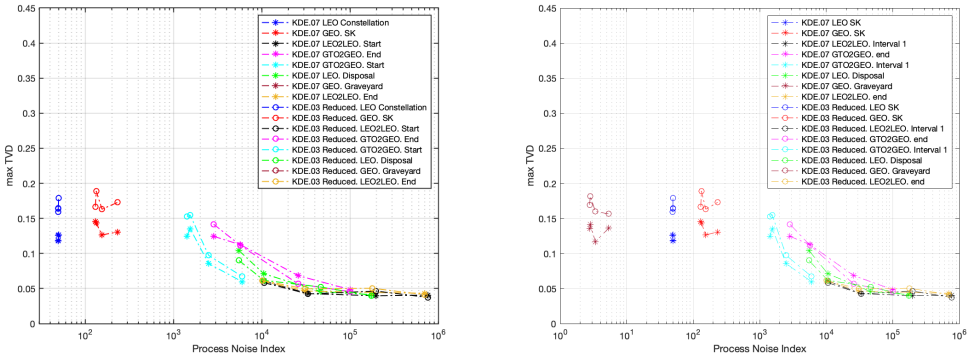

Figure 6. TVD for all combinations of scenario and process noise with KDE methods.

bits. *Journal of Guidance, Control, and Dynamics*, 44(5):983–995, May 2021.

4. J.L. Gonzalo, C. Colombo, and P. Di Lizia. A semi-analytical approach to low-thrust collision avoidance manoeuvre design. In *Proceedings of the 70th IAC*, volume October, 2019. Paper No. IAC-19-A6.2.3.
5. A. Petit, E. M. Alessi, and A. Rossi. Low-Thrust Strategies and Implications in the Perspective of Space Debris Mitigation for Large Constellations. In *First International Orbital Debris Conference*, volume 2109 of *LPI Contributions*, page 6032, December 2019.
6. P. S. Maybeck. Stochastic models, estimation, and control. In *Mathematics in Science and Engineering*, volume 141, chapter 4, pages 133–202. Elsevier, 1979.
7. A. T. Fuller. Analysis of nonlinear stochastic systems by means of the Fokker–Planck equation. *International Journal of Control*, 9(6):603–655, June 1969.
8. Yifei Sun and Mrinal Kumar. Uncertainty propagation in orbital mechanics via tensor decomposition. *Celestial Mechanics and Dynamical Astronomy*, 124(3):269–294, March 2016.
9. A. D. C. Jesus, M. L. D. O. Souza, and Antonio Prado. Statistical analysis of nonimpulsive orbital transfers under thrust errors. I. *Nonlinear Dynamics and Systems Theory*, 2, January 2002.
10. Ya-zhong Luo and Zhen Yang. A review of uncertainty propagation in orbital mechanics. *Progress in Aerospace Sciences*, 89:23–39, February 2017.
11. Richard H. Battin. *An introduction to the mathematics and methods of astrodynamics*. AIAA education series. American Institute of Aeronautics and Astronautics, New York, N.Y., 1987.
12. Arthur Gelb. *Applied Optimal Estimation*. MIT Press, Cambridge, MA, USA, April 1974.
13. S.J. Julier and J.K. Uhlmann. Unscented filtering and nonlinear estimation. *Proceedings of the IEEE*, 92(3):401–422, March 2004.
14. Ienkaran Arasaratnam and Simon Haykin. Cubature Kalman Filters. *IEEE Transactions on Automatic Control*, 54(6):1254–1269, June 2009.
15. Brandon A. Jones, Alireza Doostan, and George H. Born. Nonlinear Propagation of Orbit Uncertainty Using Non-Intrusive Polynomial Chaos. *Journal of Guidance, Control, and Dynamics*, 36(2):430–444, March 2013.
16. Ryan S. Park and Daniel J. Scheeres. Nonlinear Mapping of Gaussian Statistics: Theory and Applications to Spacecraft Trajectory Design. *Journal of Guidance, Control, and Dynamics*, 29(6):1367–1375, November 2006.

Table 4. PoC results for all scenarios given together with the number of GMEs for the primary (i.e., N_p) and secondary (i.e, N_s) objects.

Method	LEO to LEO (N_p,N_s)	LEO DISPOSAL (N_p,N_s)	LEO SK (N_p,N_s)	GTO to GEO (N_p,N_s)	GEO SK (N_p,N_s)
Linear Propagation	7.8984E-05 *(1,1)*	6.1197E-04 *(1,1)*	3.7338E-04 *(1,1)*	6.6233E-04 *(1,1)*	5.5866E-03 *(1,1)*
STM	7.8235E-05 *(15,15)*	5.9741E-04 *(15,15)*	3.6334E-04 *(15,15)*	8.9033E-04 *(15,15)*	5.4691E-03 *(15,15)*
ADAGMM	7.9897E-05 *(3,5)*	6.0673E-04 *(3,7)*	3.7008E-04 *(9,3)*	8.0935E-04 *(9,3)*	5.5866E-03 *(1,1)*
UT	1.0715E-04 *(1,1)*	6.5057E-04 *(1,1)*	3.6722E-04 *(1,1)*	2.4182E-10 *(1,1)*	2.6645E-30 *(1,1)*
RUT	1.0752E-04 *(1,1)*	6.4990E-04 *(1,1)*	3.6914E-04 *(1,1)*	3.7664E-12 *(1,1)*	1.0992E-30 *(1,1)*
SRC3	1.0801E-04 *(1,1)*	6.5131E-04 *(1,1)*	3.6980E-04 *(1,1)*	1.7747E-12 *(1,1)*	1.0860E-30 *(1,1)*
SRC5	1.0782E-04 *(1,1)*	6.5056E-04 *(1,1)*	3.7017E-04 *(1,1)*	1.0210E-12 *(1,1)*	6.8515E-31 *(1,1)*
KDE	7.6399E-05 *(20,20)*	6.4632E-04 *(20,20)*	3.8714E-04 *(20,20)*	1.8271E-12 *(20,20)*	5.2736E-32 *(20,20)*
MC	- *(-,-)*	- *(-,-)*	- *(-,-)*	7.6273E-04 *(-,-)*	5.0727E-03 *(-,-)*

17. K. Fujimoto, D. J. Scheeres, and K. T. Alfriend. Analytical Nonlinear Propagation of Uncertainty in the Two-Body Problem. *Journal of Guidance, Control, and Dynamics*, 35(2):497–509, March 2012.
18. Martin Berz. Differential Algebraic Techniques. In *Advances in Imaging and Electron Physics*, volume 108, pages 81–117. Elsevier, 1999.
19. M. Valli, R. Armellin, P. Di Lizia, and M. R. Lavagna. Nonlinear Mapping of Uncertainties in Celestial Mechanics. *Journal of Guidance, Control, and Dynamics*, 36(1):48–63, January 2013.
20. O Montenbruck and E Gill. Satellite Orbits: Models, Methods, and Applications. *Applied Mechanics Reviews*, 55(2):B27–B28, April 2002.
21. Gabriel Terejanu, Puneet Singla, Tarunraj Singh, and Peter D. Scott. Uncertainty Propagation for Nonlinear Dynamic Systems Using Gaussian Mixture Models. *Journal of Guidance, Control, and Dynamics*, 31(6):1623–1633, November 2008.
22. Kyle J. DeMars, Robert H. Bishop, and Moriba K. Jah. Entropy-Based Approach for Uncertainty Propagation of Nonlinear Dynamical Systems. *Journal of Guidance, Control, and Dynamics*, 36(4):1047–1057, July 2013.
23. Vivek Vittaldev and Ryan P. Russell. Space Object Collision Probability Using Multidirectional Gaussian Mixture Models. *Journal of Guidance, Control, and Dynamics*, 39(9):2163–2169, September 2016.
24. Zhen-Jiang Sun, Ya-Zhong Luo, Pierluigi Di Lizia, and Franco Bernelli Zazzera. Nonlinear orbital uncertainty propagation with differential algebra and Gaussian mixture model. *Science China Physics, Mechanics, and Astronomy*, 62:34511, March 2019.
25. Alberto Fossà, Roberto Armellin, Emmanuel Delande, Matteo Losacco, and Francesco Sanfedino. Multifidelity Orbit Uncertainty Propagation using Taylor Polynomials. In *AIAA SCITECH 2022 Forum*, San Diego, CA & Virtual, January 2022. American Institute of Aeronautics and Astronautics.
26. Michele Maestrini, Andrea De Vittori, Pierluigi Di Lizia, and Camilla Colombo. Dynamics-based uncertainty propagation with low-thrust. In *2022 AAS/AIAA Astrodynamics Specialist Conference, 7-11 August, 2022, Charlotte, North Carolina*, pages 1–20. AIAA, 2022. Paper No. AAS 22-634.
27. Mirco Rasotto, Alessandro Morselli, Alexander Wittig, Mauro Massari, Pierluigi Di Lizia, Roberto Armellin, Celia Valles, and Guillermo Ortega. Differential algebra space toolbox for nonlinear uncertainty propagation in space dynamics. In *The 6th International Conference on Astrodynamics Tools and Techniques (ICATT) (14/03/16 - 17/03/16)*, March 2016.
28. Leandro Pardo. *Statistical inference based on divergence measures*, chapter 1, page 51. Chapman and Hall/CRC, 2018.
29. John L. Junkins, Maruthi R. Akella, and K. Terry Alfriend. Non-gaussian error propagation in orbital mechanics. *Journal of The Astronautical Sciences*, 44:541–563, 1996.
30. Alexander Wittig, Pierluigi Di Lizia, Roberto Armellin, Kyoko Makino, Franco Bernelli-Zazzera, and Martin Berz. Propagation of large uncertainty sets in orbital dynamics by automatic domain splitting. *Celestial Mechanics and Dynamical Astronomy*, 122(3):239–261, Jul 2015.
31. Bernt Øksendal. *Stochastic differential equations, 6th edition*. Springer, 2007.

32. Lawrence C Evans. *An introduction to stochastic differential equations*, volume 82. American Mathematical Soc., 2012.
33. W Rüemelin. Numerical treatment of stochastic differential equations. *SIAM Journal on Numerical Analysis*, 19(3):604–613, 1982.
34. Peter E Kloeden and Eckhard Platen. *Numerical solution of stochastic differential equations*. Springer, 1995.
35. Kristian Debrabant. Runge-Kutta methods for third order weak approximation of SDEs with multidimensional additive noise. *BIT Numerical Mathematics*, 50(3):541–558, 2010.
36. Richard H Battin. *An introduction to the mathematics and methods of astrodynamics*. Aiaa, 1999.
37. G Porcelli and E Vogel. Two-impulse orbit transfer error analysis via covariance matrixgel. *Journal of Spacecraft and Rockets*, 17(3):248–255, 1980.
38. Prabhakara P Rao and Stephen C Bell. Conditional performance error covariance analyses for commercial titan launch vehicles. *Journal of guidance, control, and dynamics*, 14(2):398–405, 1991.
39. Robert A LaFarge and Roy S Baty. Functional dependence of trajectory dispersion on initial condition errors. *Journal of Spacecraft and Rockets*, 31(5):806–813, 1994.
40. Arthur Gelb et al. *Applied optimal estimation*. MIT press, 1974.
41. S. J. Julier and J. Uhlmann. Unscented filtering and nonlinear estimation. *Proceedings of the IEEE*, 92(2):401–422, March 2004.
42. Ya-zhong Luo and Zhen Yang. A review of uncertainty propagation in orbital mechanics. *Progress in Aerospace Sciences*, 89:23–39, 2017.
43. C Yanez, M Gupta, V Morand, and JC Dolado. On the gaussianity validity time for orbital uncertainty propagation. In *ESA NEO and debris detection conference, Darmstadt, Germany*, 2019.
44. Bin Jia, Ming Xin, and Yang Cheng. High-degree cubature kalman filter. *Automatica*, 49(2):510–518, 2013.
45. Bin Jia and Ming Xin. Orbital uncertainty propagation using positive weighted compact quadrature rule. *Journal of Spacecraft and Rockets*, 54(3):683–697, 2017.
46. Henrique MT Menegaz, João Y Ishihara, Geovany A Borges, and Alessandro N Vargas. A systematization of the unscented Kalman filter theory. *IEEE Transactions on Automatic Control*, 60(10):2583–2598, 2015.
47. B. Ristic, S. Arulampalam, and N. Gordon. *Beyond the Kalman Filter: Particle Filters for Tracking Applications*. Artech House, Boston, 2004.
48. Sanat K Biswas, Ben Southwell, and Andrew G Dempster. Performance analysis of fast unscented kalman filters for attitude determination. *IFAC-PapersOnLine*, 51(1):697–701, 2018.
49. Naoya Ozaki, Stefano Campagnola, Ryu Funase, and Chit Hong Yam. Stochastic differential dynamic programming with unscented transform for low-thrust trajectory design. *Journal of Guidance, Control, and Dynamics*, 41(2):377–387, 2018.
50. Marco Martorella. Optimized tracking of low thrust orbit raising maneuvers. Technical report, CONSORZIO NAZIONALE INTERUNIVERSITARIO PER LE TELECOMUNICAZIONI, 2020.
51. Yu Wang, Chao Han, and Xiucong Sun. Optimization of low-thrust earth-orbit transfers using the vectorial orbital elements. *Aerospace Science and Technology*, 112:106614, 2021.
52. Boris Benedikter, Alessandro Zavoli, Zhenbo Wang, Simone Pizzurro, and Enrico Cavallini. Covariance control for stochastic low-thrust trajectory optimization. In *AIAA SCITECH 2022 Forum*, page 2474, 2022.
53. I. Arasaratnam and S. Haykin. Cubature kalman filters. *IEEE Transactions on Automatic Control*, 54(6):1254–1269, 2009.
54. Juan-Carlos Santos-León, Ramón Orive, Daniel Acosta, and Leopoldo Acosta. The cubature Kalman filter revisited. *Automatica*, 127:109541, 2021.
55. Gabriel Terejanu, Puneet Singla, Tarunraj Singh, and Peter D Scott. Uncertainty propagation for nonlinear dynamic systems using gaussian mixture models. *Journal of guidance, control, and dynamics*, 31(6):1623–1633, 2008.
56. B. W. Silverman. *Density Estimation for Statistics and Data Analysis*. Chapman & Hall/CRC, Boca Raton (FL, USA), 1986.
57. M. P. Wand and M. C. Jones. *Kernel Smoothing*. Chapman-Hall/CRC, 1995.
58. D. Crisan and J. Miguez. Nested particle filters for online parameter estimation in discrete-time state-space markov models. *arXiv*, 1308.1883v2 [stat.CO], 2014.
59. L. G. Jacchia. Thermospheric Temperature, Density, and Composition: New Models. *SAO Special Report*, 375, March 1977.
60. Ken Chan. Improved analytical expressions for computing spacecraft collision probabilities. *Advances in the Astronautical Sciences*, 114:1197–1216, 2003.
61. Paul Dagum, Richard Karp, Michael Luby, and Sheldon Ross. An optimal algorithm for monte carlo estimation. *SIAM Journal on Computing*, 29(5):1484–1496, 2000.